

BASIS FOR THE THERMAL-VACUUM HOT DWELL TEST DURATION

James Fu, Senior Engineer and Member of Technical Staff
Environmental and Reliability Engineering
Jet Propulsion Laboratory, Pasadena, Ca

Abstract: Of all the parameters involved in an assembly-level thermal-vacuum test, hot dwell test duration is the one element that is long standing, but least discussed and least understood. By drawing upon methods from reliability and physics, this paper presents the motivation, rationale, and basis for thermal-vacuum hot dwell test durations. It is proposed in this work to use the best-fit statistical model from reliability, namely, Weibull, exponential, normal, or lognormal base e, etc., to determine the distribution of early test failures. The resulting hazard functions (i.e., instantaneous failure rates) and their rates of change are then used to derive the proper dwell durations. This methodology is applied to life test data for piece parts such as Vishay-Sprague capacitors, CMOS, etc., and the environmental test failure data from flight assemblies such as those of Mariner 69, Voyager77, Galileo89, and Cassini97 spacecrafts. The results are presented. This paper also presents the review, re-formulation, and re-interpretation of molecular venting, outgassing, curing, and stress relaxation as they are related to the hot dwell test durations. The results show that, in order for the rate of instantaneous failure (hazard function) reduction to reach the level of $-6.0E-06$ 1/hour², the hot test duration varies from 25 hours for the Vishay Sprague Tantalum Capacitors to 76 hours for Mariner69 spacecraft assemblies. The studies of physical phenomena show that hot test durations range from 20 hours for the completion of molecular venting to 80 hours for that of stress relaxation. This work suggests that the hot dwell duration for each test should be determined in two steps: (1) A minimum hot duration of 80 hours be required; and then followed by (2) Specific tailoring be conducted to arrive at the proper test duration.

Key words: early test failure distribution, Weibull analysis, related physics, hot dwell test durations

1. Motivation

For Mariner 64, 67, 69, 71, 73 and Viking 75 spacecrafts, JPL's environmental programs required long hot dwell test durations (up to 288 hours) for assembly-level qualification thermal vacuum tests. Voyager77 spacecrafts had a combination of 288 hour and 144 hour hot dwell test durations. Galileo 89, Magellan 89, Wide-Field Planetary Cameras 90 & 93, Cassini 97, and other spacecrafts and instruments had 144 hour hot test durations.

Many attempts have been made to rationalize the 144 hours test duration or, otherwise, shorten it. JPL Thermal Environmental Group's "Red Book", the "fit.f" computer program, Long-Life/High Reliability Design Guidelines, Test Effectiveness Studies were

a few examples of such efforts. The Voyager failure data, in particular, have been studied by numerous investigators.

The obstacles for the progress to shorten the test durations are many folds:

- The lack of suitable data – Ideal data is almost non-existent. Available data were either of limited sample size or unsuitable for statistical analysis.
- The lack of multi-disciplined personnel who are skillful with the tools of physics, reliability, statistics, and testing.
- The belief that the test duration as a test parameter is inherently arbitrary and subjective and, therefore, cannot be subjected to rationalization.
- The lack of tools themselves. For instance, the statistical software package was not available to JPL Environmental Group until this year.

Mars Climatic Orbiter, Mars Polar Lander, and Mars Exploration Rover (MER) Projects prompted the re-evaluation of spacecraft design rules and testing standards. The effort on the rationalization of the hot test duration is thus renewed. Several recent events prompted the revisit of the methodology and analytical tools for the hot test duration as a test parameter and, therefore, the preparation of this paper:

- (1) The initiation of the document “Environmental Assurance Handbook – Temperature Test Requirements Rationale”.
- (2) The availability of the Vishay-Sprague Tantalum capacitor life test data.
- (3) The purchase of “Minitab” Statistical Analysis Software Package [1].

2. Methods from Reliability and Physics

For N_0 units under test, $N_f(t)$ units have failed at time t . The cumulative failure distribution function of the units under test can be expressed as [2]:

$$F(t) = N_f(t)/N_0$$

$F(t)$ is seen to be a simple ratio and is, therefore, sometimes described as the cumulative fractions of the failures of the units under test (at time t).

If parametric study indicates that $F(t)$ data fits well with the two-parameter Weibull distribution model with shape parameter β and scale parameter η , then the cumulative distribution function is said to be expressible by the relationship:

$$F(t) = 1.0 - e^{-(t/\eta)^\beta}$$

and its related quantities are:

$$\text{Reliability Function: } R(t) = 1 - F(t) = e^{-(t/\eta)^\beta}$$

$$\text{Probability Density Function } p(t) = F'(t) = (\beta/\eta)(t/\eta)^{\beta-1}(e^{-(t/\eta)^\beta})$$

$$\text{Hazard Function } h(t) = p(t)/R(t) = (\beta/\eta)(t/\eta)^{\beta-1}$$

Reliability function, $R(t)$, is the probability that the unit will survive until time t . The probability density function, $p(t)$, corresponds to a histogram of the life times of the population. Hazard function, $h(t)$, is oftentimes referred to as the instantaneous failure rate. The product $\{h(t)dt\}$ represents that proportion of the remaining population which will fail in the time interval between t and $t+dt$. It is a measure of the “proneness” to failure of the units.

Based on available failure and survival data, the task at hand is to estimate the parameters β and η and to gauge whether the data support the assumption of an underlying Weibull distribution or other possible distribution, such as normal, lognormal, exponential, or extreme value.

In determining the proper hot dwell test duration, the criterion used in this work is:

The rate of change of hazard function, dh/dt , $< \epsilon$
where ϵ is a certain small value

The “driving force” which prompted the failures of the parts is to be reduced to a certain level before the test should be stopped. The rate of change of hazard function (“the acceleration”), rather than the hazard function itself (“the velocity”), is considered appropriate for this purpose. The rate of change of hazard function:

$$dh/dt = -6.00E-06 \text{ 1/hour}^2$$

is chosen as the point of diminishing return.

Ideally,

All N_0 starting units are identical (i.e., design, shape, materials, processes, ..., etc.)

N_0 is a very large number;

All test conditions are identical (i.e., handling, temperatures, pressures, humidities, wattages, stresses,....etc.);

No parts have been burned in;

No operating hours have been accumulated;

No distinction is made of the different failure mechanisms
etc.

Realistically, however, these conditions are never met. JPL spacecraft assemblies do not meet these requirements. Suppliers' parts do not.

If one forces the issue and imposes the following restrictions on the spacecraft assemblies and their failures:

- Limit "failures" to workmanship defects;
- Limit failures to faults of "processes" such as soldering, assembling, welding, interfacing, interconnects, fittings, connectors, etc.;
- Makes no distinction between parts or assembly failures;
- Makes no distinction between qualification and acceptance tests;
- Be flexible about test temperature levels;

but excludes:

- Failures occurred on developmental units;
- Human or operator errors;
- Software errors;
- Facility or test equipment failures,

maybe spacecraft assemblies can be subjected to statistical modeling and the derivation of the reasonable hot dwell test duration.

Also, in the ultimate, basic physics should govern the behavior of the assembly under hot dwell testing. Basic physics should provide pertinent clues for the duration of hot dwell testing.

3. Tantalum Capacitors

Vishay Sprague tantalum capacitor life test data from Ref. [3] is summarized in Table 3-1. Data for three original tests and two re-tests on capacitors from two lots are shown. The data were recorded for a total of 3129 capacitors with 577 failed capacitors before the tests were terminated. The acceleration factors [4], actual failure times, rated failure times (acceleration factor times the actual failure time), and the censorship indicators are all shown in Table 3-1.

Statistical software package Minitab [1] was used to perform the parametric distribution analysis. Maximum likelihood estimation and right-censoring technique were used in the analysis. For comparison purposes, the data were fitted to eight distribution models and the results are shown in Figure 3-1. Weibull, lognormal base e, exponential, normal, lognormal base 10, extreme value, loglogistic, and logistic models were attempted. As

Table 3-1. Vishay-Sprague WPB CWR09 Tantalum Capacitor Life Test Data [3]

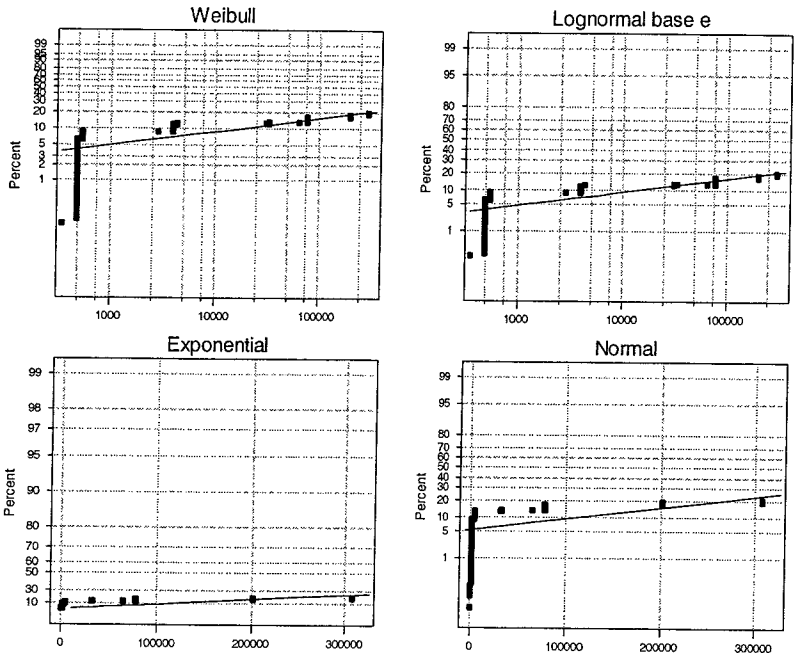
Lot	Initial Qty	Accel. Factor	Measured Failure Time (hrs)	Rated Failure Time, t (hrs)	No. of Parts Failed @ t	Cap. (μ f)	Censor Flag	Comments
9815L003	2007	1924.91	0.25	481.23	150	6.8	0	Original Test
"	"	"	2.00	3849.82	88	"	0	
"	"	"	40.00	76996.40	95	"	0	
"	"	"	160.00	307985.60	28	"	0	
"	"	"	160.00	307985.60	1646	"	1	
"	103	1395.24	0.25	348.81	1	"	0	Retest
"	"	"	2.00	2790.48	2	"	0	
"	"	"	6.35	8859.77	0	"	0	
"	"	"	23.50	32788.14	3	"	0	
"	"	"	30.80	42973.39	0	"	0	
"	"	"	46.20	64460.09	1	"	0	
"	"	"	46.20	64460.09	96	"	1	
0013L003	519	2142.88	0.25	535.72	82	"	0	Original Test
"	"	"	2.00	4285.76	13	"	0	
"	"	"	94.00	201430.72	48	"	0	
"	"	"	94.00	201430.72	376	"	1	
"	400	1924.91	0.25	481.23	39	"	0	Original Test
"	"	"	2.00	3849.82	11	"	0	
"	"	"	16.00	30798.56	12	"	0	
"	"	"	16.00	30798.56	338	"	1	
"	100	0.90	0.25	0.23	1	"	0	Retest
"	"	"	2.00	1.80	1	"	0	
"	"	"	15.70	14.13	2	"	0	
"	"	"	15.70	14.13	96	"	1	

shown in Figure 3-1, the Anderson & Darling goodness-of-fit indicators all had values of about 9600, large by conventional standards.

The analysis was carried forward on account of consistency. Analyses with multiple failure mechanisms (i.e., separate analyses for different time zones and slopes) were not performed for the following reasons:

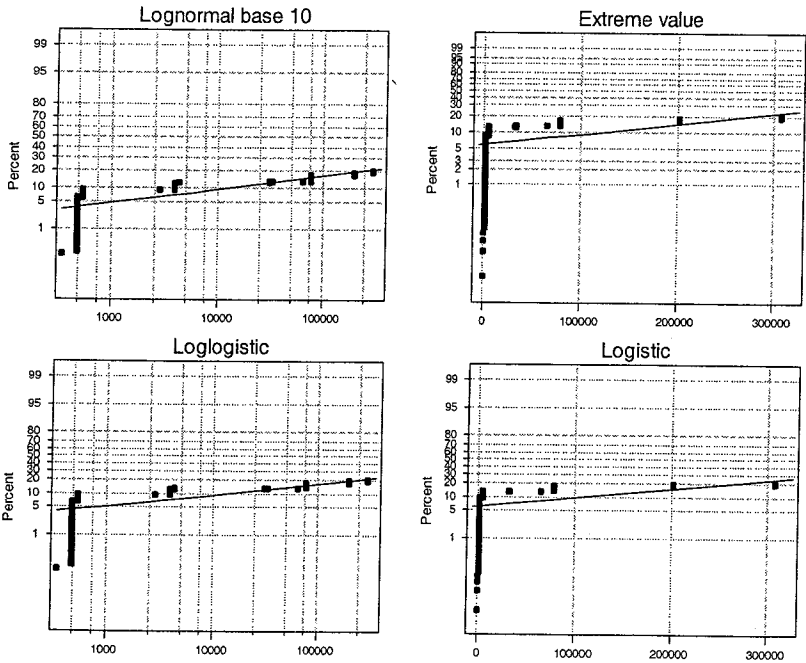
- (1) The Weibull distribution is a commonly used reliability estimation tool even though the result is not mathematically rigorous.
- (2) The accuracy of the fit may not be important for the study of the behavior of early failures.
- (3) The integrity and simplicity of the data need to be preserved; subjective manipulation of the data is to be avoided.
- (4) One consistent method is needed for comparison with analyses of failure data for other parts and assemblies.

Four-way Probability Plot for capacitors ML Estimates - Censoring Column in Censor



- Anderson-Darling (adj)
- Weibull 9604
 - Lognormal base e 9604
 - Exponential 9635
 - Normal 9606

Four-way Probability Plot for capacitors ML Estimates - Censoring Column in Censor



- Anderson-Darling (adj)
- Lognormal base 10 9604
 - Extreme value 9606
 - Loglogistic 9604
 - Logistic 9606

Figure 3-1. Fitting of the Vishay-Sprague Tantalum Capacitor Data

Weibull distribution was chosen for further analysis. The resulting parameters were found to be:

- Shape factor, $\beta = 0.2659$
- Scale factor, $\eta = 7.25E07$ hours
- MTTF (mean time to failure) = $1.22E09$ hours
- Standard Deviation = $8.69E09$ hours
- Median = $1.827E07$ hours
- Inter-Quartile-Range = $2.47E08$ hours

The calculated probability density function, probabilities of failure, survival (reliability) function, and hazard function are shown in Figure 3-2 along with the 95% confidence intervals.

The rate of change of hazard function for the tantalum capacitors was calculated utilizing the Weibull shape and scale factors and the results are shown in Figure 3-3. The rate of change of hazard function reaches $-6.0E-06$ 1/hour² at the 25th hour. This time, therefore, is considered to be the proper duration for a thermal vacuum hot dwell test for the tantalum capacitors.

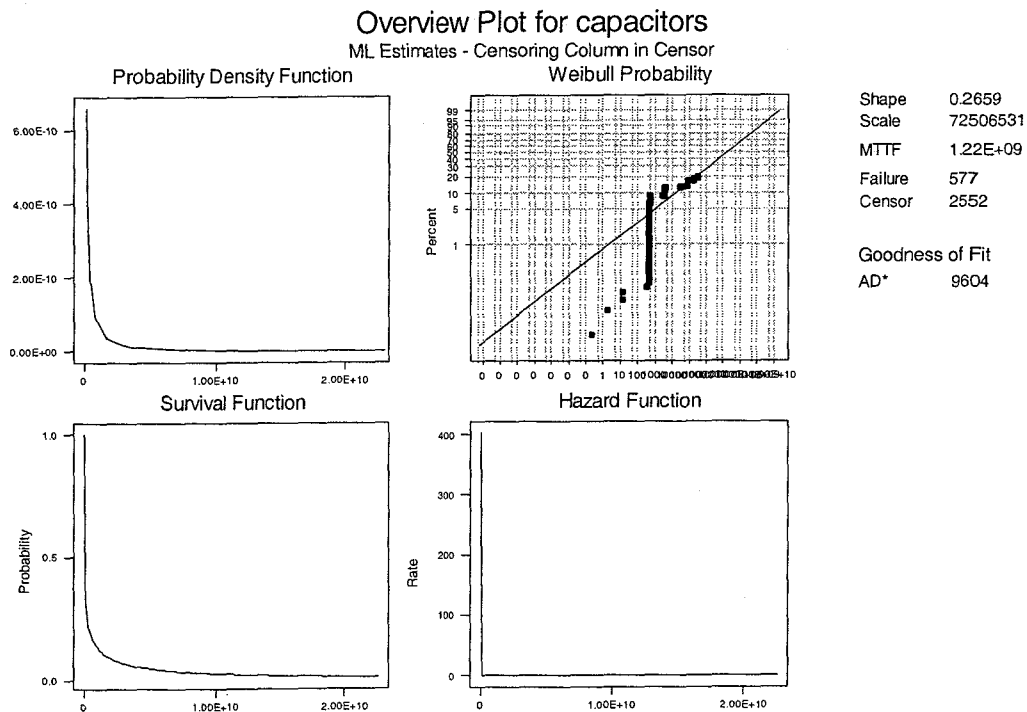


Figure 3-2a. Weibull Representation of the Vishay-Sprague Capacitor Data

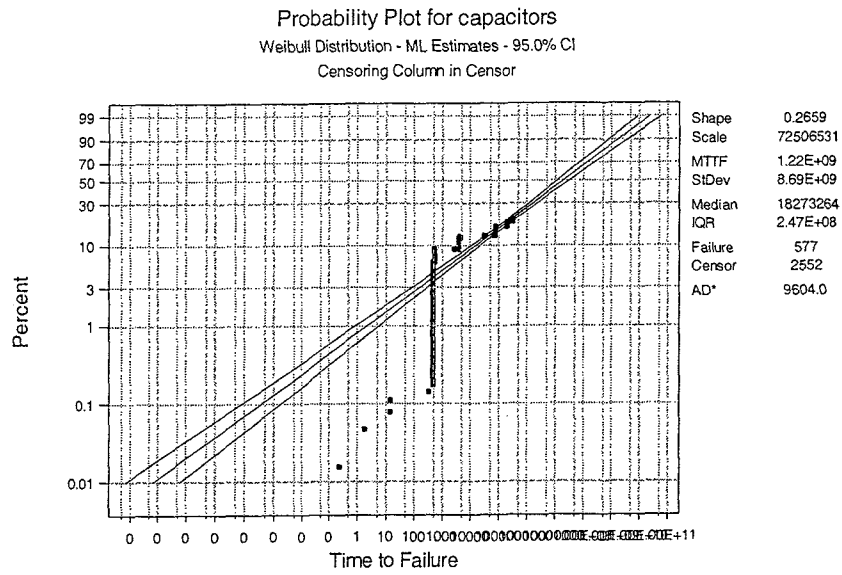


Figure 3-2b. Weibull Representation of the Vishay-Sprague Capacitor Data

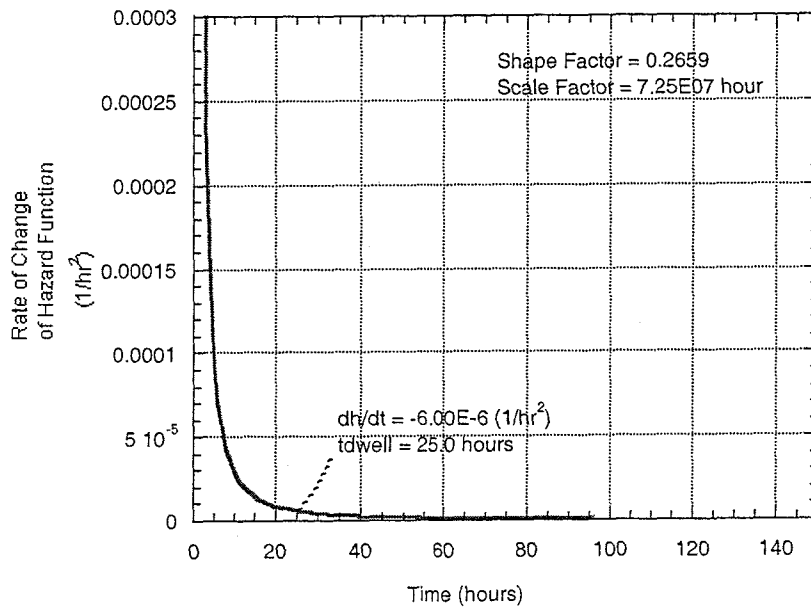


Figure 3-3. Rate of Change of Hazard Function – Vishay-Sprague Capacitors

4. CMOS IC's

Basic Elements of CMOS Devices

The basic elements of a CMOS device are shown in Figure 4-1 below. They consist of:

- (1) The Tantalum Silicide (TaSi_2)/Poly-Silicon Electrode
- (2) The Thin Oxide film
- (3) The Field Oxide (as Isolation)
- (4) The Substrate
- (5) The Leads

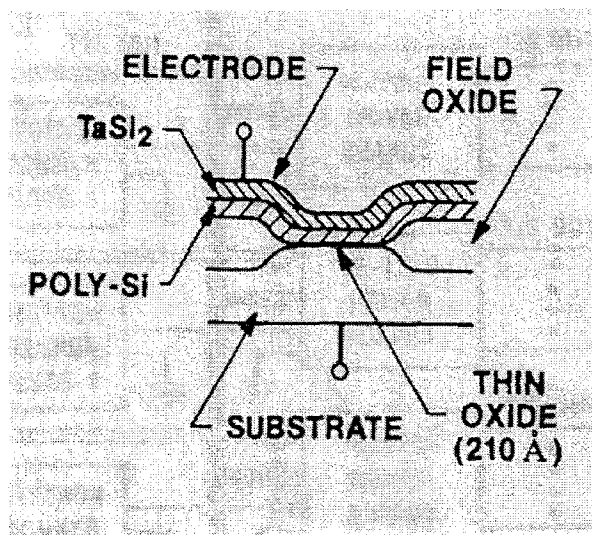


Figure 4-1. Elements of CMOS
After Boyko and Gerlach [6]

In their experiment, Boyko and Gerlach [6] used oxide films of 21 nanometers in thicknesses (i.e., 210 Angstroms).

Failure Mechanisms of CMOS

CMOS usually fails due to one of three failure mechanisms:

- (1) Electromigration in the Traces: Electromigration is the unwanted movements of the metal grains in the trace caused by the impacts of electrons. It is usually the result of random inhomogeneities in the microstructure of the traces. The probability of this failure is typically high but related with higher electric fields and temperatures only.

- (2) Hot Carriers: Hot carriers are the electrons that have gained high energies in the presence of high electric fields. These high-energy electrons, when trapped in the gate oxides of CMOS devices, degrade the performance of the device and, in severe cases, cause failure of the device.
- (3) Oxide Breakdown: Oxide breakdown is the electric shorting resulting from the random local thinning of the oxide film due to imperfections in the manufacturing processes. The probability of oxide breakdown is normally low.

Failure Modes of Oxide Film

Of the three failure mechanisms of CMOS devices described above, oxide breakdown is the most likely for normal operating conditions. That is, oxide breakdown is usually the cause of failure of CMOS when the electric fields, application temperatures, and the current densities are in the normal ranges of operations. Oxide breakdown has two distinctive failure “modes”:

- (1) Intrinsic mode occurs at higher E-field. It represents breakdown of the intrinsic breakdown strength of the oxide. For normal operating conditions and oxides film thicknesses between 20 and 25 nanometers, intrinsic breakdown does not occur as early failures [7].
- (2) Defect mode, as the name implies, is the defect-related failure mode and is normally induced by imperfect manufacturing processes. It is caused by random localized “thin spots” or “pinholes”. Stress cracks, asperities, silicon lattice defects, particulate microcontamination and local interface problems can all be the cause of defect breakdown [6]. Defect breakdown can occur at lower stress levels and as early life failures of the CMOS device.

CMOS Oxide Film Life Test Data

The device developed for the oxide film testing by Boyko and Gerlach [6] is shown in Figure 4-2 below.

The test device was in the form of a structural coupon. The overall area was 0.74 cm^2 (0.200 inch by 0.575 inch). The total thin oxide active area was 0.3 cm^2 . The sample size was quite large ($N_o = 14000$); that is, 14000 thin oxide films representing a mature $1.25 \mu\text{m}$ CMOS process were tested. The failure criterion for the test was that the leak current must not exceed $10 \mu\text{A}$.

The stress factors used in the test were:

Temperature = $150 \text{ }^\circ\text{C}$ (uncorrected to $75 \text{ }^\circ\text{C}$ due to insensitivity [6])
Field Strength = 4.0 MV/cm (close to operating field strengths)

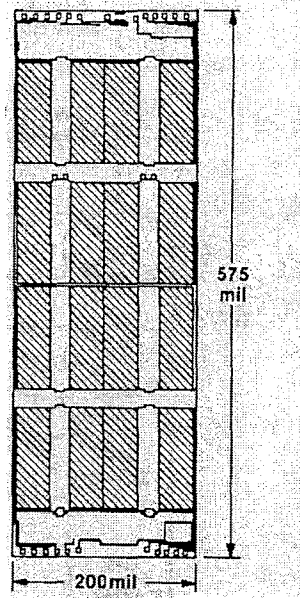


Figure 4-2. Test Device of Boyko and Gerlach [6]

The numerical data of Boyko and Gerlach [6] and its interpretation by Buehler [7] is shown in Table 4-1. The same data is shown graphically in Figure 4-3.

The test data, as shown, is for the dielectric defect breakdown only since dielectric breakdown is most likely to be uncovered in a thermal vacuum hot test. The data is shown in the form of failure times in hours and probability of failure in fractions. Area correction was not performed due to insensitivity [6]

Reliability and Survivability Analysis of the CMOS Data

The CMOS oxide breakdown test data [6] was analyzed in an identical manner as that performed for the tantalum capacitors. The results of the analysis are shown in Figure 4-4. Probability of failure, probability density function, the survivability function, and the hazard function are shown along with the Mean Time To Failure (MTTF), goodness of fit, and sample size.

Table 4-1. CMOS Oxide Film Failure Data of Boyko and Gerlach [6], [7]

time t (hours)	probability of failure	cumulative number of failures	number of failures at time t	right censor flag	remarks
0.0018	0.05	700	700	0	exact data
0.002	0.06	840	140	0	
0.0026	0.065	910	70	0	
0.0044	0.071	994	84	0	
0.014	0.075	1050	56	0	
0.017	0.076	1064	14	0	
0.021	0.079	1106	42	0	
0.033	0.08	1120	14	0	
0.045	0.081	1134	14	0	
0.047	0.082	1148	14	0	
0.049	0.083	1162	14	0	
0.051	0.084	1176	14	0	
0.28	0.086	1204	28	0	
0.3	0.088	1232	28	0	
0.32	0.09	1260	28	0	
0.58	0.091	1274	14	0	
0.89	0.092	1288	14	0	
0.9	0.096	1344	56	0	
1.1	0.099	1386	42	0	
1.4	0.1	1400	14	0	
1.7	0.101	1414	14	0	
2.2	0.102	1428	14	0	
3.2	0.105	1470	42	0	
4.5	0.107	1498	28	0	
4.7	0.108	1512	14	0	
5	0.112	1568	56	0	
5.1	0.113	1582	14	0	
8.1	0.116	1624	42	0	
8.2	0.117	1638	14	0	
11	0.119	1666	28	0	
11.5	0.119	1666	0	0	
18	0.12	1680	14	0	
19	0.125	1750	70	0	
22	0.13	1820	70	0	
24	0.135	1890	70	0	
27	0.138	1932	42	0	
36	0.14	1960	28	0	
39	0.14	1960	0	0	
45	0.14	1960	0	0	
58	0.141	1974	14	0	
61	0.142	1988	14	0	
64	0.142	1988	0	0	
64	1	14000	12012	1	censored data

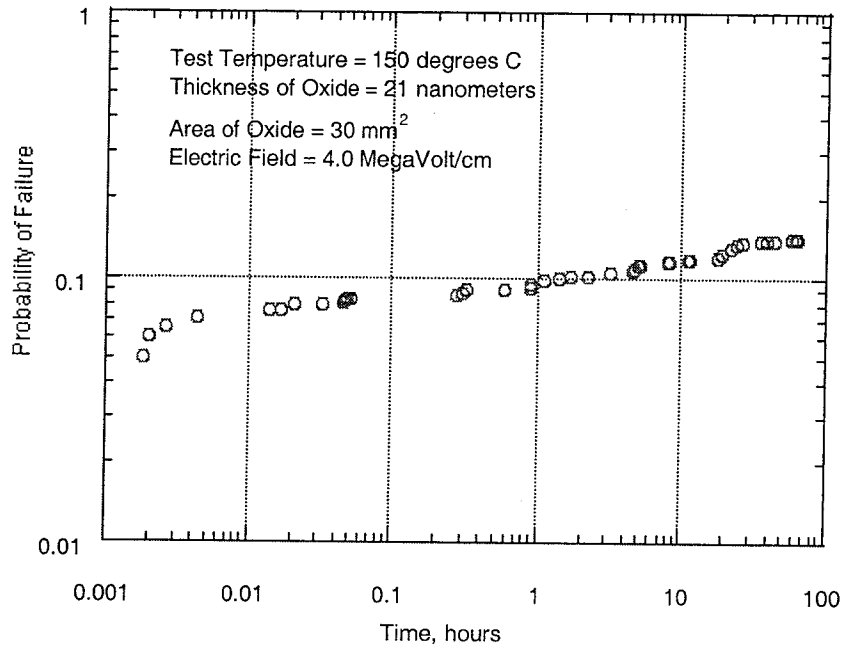


Figure 4-3. CMOS Oxide Breakdown Test Data – Boyko and Gerlach, 1989 [6], [7]

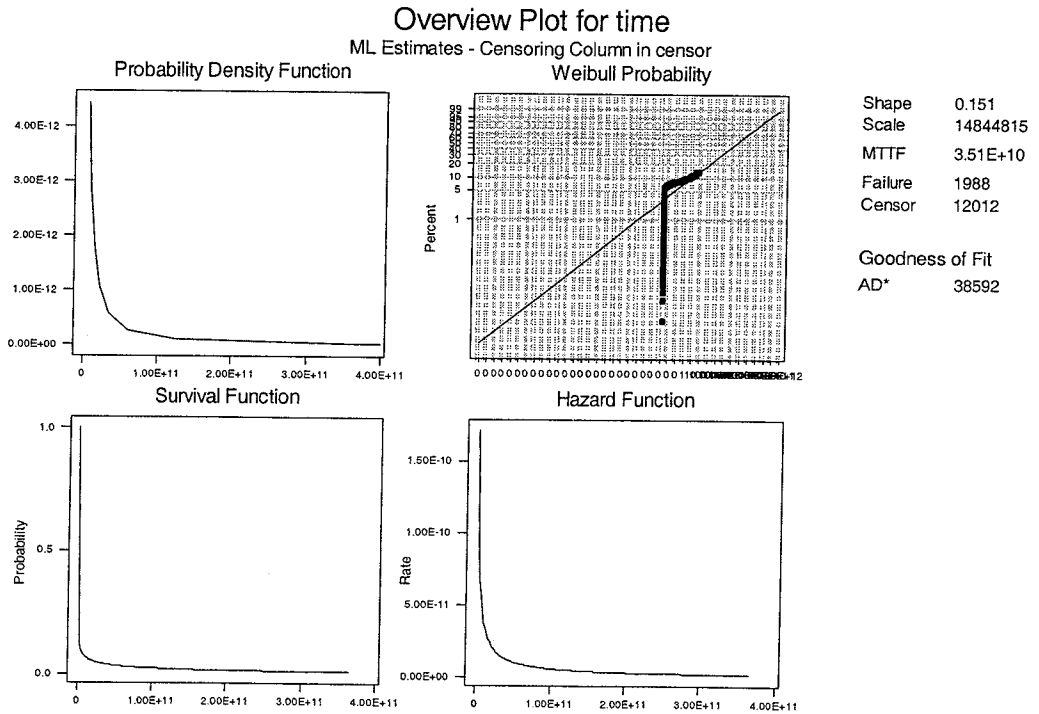


Figure 4-4. Probability of Failures, Probability Density Function, Survivability Function, and Hazard Function of CMOS Oxide Film Test Data by Boyko and Gerlach [6]

Thermal Vacuum Hot Dwell Test Duration

The rate of change of hazard function was calculated and is shown in Figure 4-5.

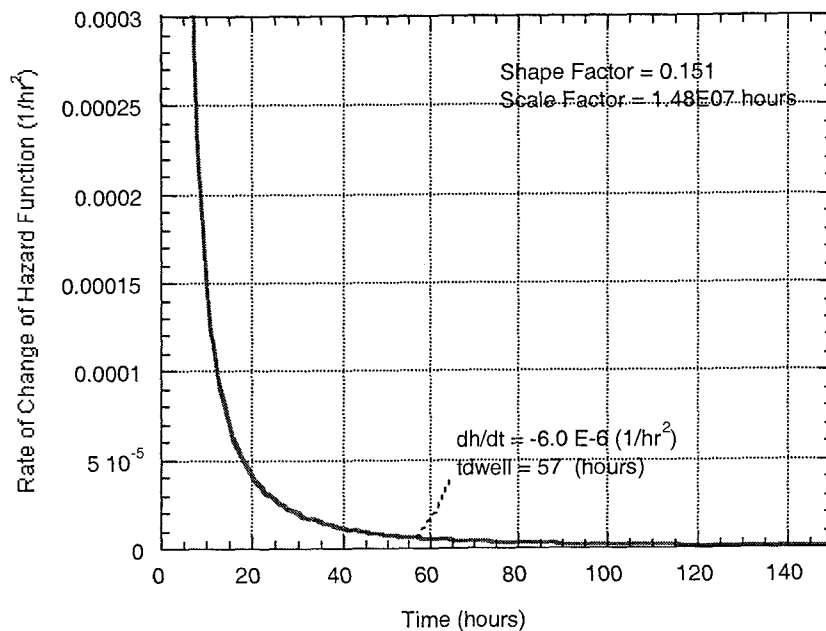


Figure 4-5. Rate of Change of Hazard Function –
Data of Boyko and Gerlach [6]

The criterion for the proper duration of thermal vacuum hot dwell test is:

$$dh/dt < \text{or} = 6.0 \times 10^{-6} \text{ (1/hr}^2\text{)}$$

That is, the change of the instantaneous failure rate of the article under test must be lower than $6.0 \times 10^{-6}/\text{hour}^2$ before the test should be terminated. This criterion is consistent with those used for analyses of data for other parts and assemblies.

Based on this criterion, the CMOS oxide film data of Boyko and Gerlach [6] indicates that the thermal vacuum hot dwell test duration should be

$$\tau_{\text{dwell}} = 57 \text{ hours}$$

As indicated in Figure 4-5, this is considered to be the proper duration for the hot dwell test whether the CMOS device or the oxide film is considered as a stand-alone part under test or as one of the components comprising the assembly under test.

As indicated in the figure, the data has the following characteristics:

- The test failures included those from the qualification, flight acceptance, and retests
- Test temperature ranged from $-20\text{ }^{\circ}\text{C}$ to $+75\text{ }^{\circ}\text{C}$ for qualification tests and $0\text{ }^{\circ}\text{C}$ to $+55\text{ }^{\circ}\text{C}$ for flight acceptance tests.
- The tests were terminated at the end of 144 hours or 288 hours.

The proposed method of analysis can, therefore, only be loosely applied to the Voyager data. Altogether, assembly test failure data from four spacecrafts are presented in Table 5-1:

Mariner69
 Voyager77
 Galileo89
 Cassini97

The available details of the data are retained in JPL's Automated Problem/Failure Data System [8] and the personal files of the author of this work [9]. The data for the statistical analyses are shown in Table 5-1. The times of failures, the number of failures at each time of observation, and the right-censorship are shown.

Table 5-1. Spacecraft Assembly Hot Dwell Test Failure Data [8], [9]

Mariner 69			Voyager77			Galileo89			Cassini97		
time	freq	censor	time	freq	censor	time	freq	censor	time	freq	censor
1.00	1	0	44.00	1	0	64	1	0	84.00	1	0
3.00	1	0	202.45	1	0	83	1	0	144.00	1	0
11.00	1	0	93.30	1	0	58	1	0	66.20	1	0
20.00	1	0	130.80	1	0	143	1	0	144.00	1	0
22.00	1	0	72.00	1	0	4	1	0	162.00	1	0
24.00	1	0	255.60	1	0	15.5	1	0	144.00	1	0
25.00	1	0	132.00	1	0	32	1	0	144.00	1	0
50.00	1	0	10.90	1	0	48	1	0	144.00	1	0
98.00	1	0	256.70	1	0	10	1	0	144.00	1	0
114.00	1	0	16.00	1	0	144	1	0	24.00	1	0
146.00	1	0	0.04	1	0	68	1	0	86.00	1	0
170.00	1	0	60.80	1	0	25	1	0	144.00	1	0
201.00	1	0	121.37	1	0	32	1	0	144.00	1	0
212.00	1	0	93.50	1	0	84	1	0	8.00	1	0
230.00	1	0	333.30	1	0	48	1	0	0.01	1	0
276.00	1	0	130.00	1	0	168	1	0	6.00	1	0
288.00	44	1	207.90	1	0	32	1	0	60.00	1	0
			144.00	22	1	20	1	0	144.00	80	1
			288.00	21	1	88	1	0			
						144	88	1			

The test failure data of each spacecraft is subjected to the same method of analysis as that for the Vishay Sprague Capacitors, except that only Weibull distribution of failure is used. The fits of the data with the Weibull distribution model are graphically shown in Figure 5-2. It is seen that the fits are significantly better than those for the Vishay Sprague capacitors and the CMOS oxide breakdown.

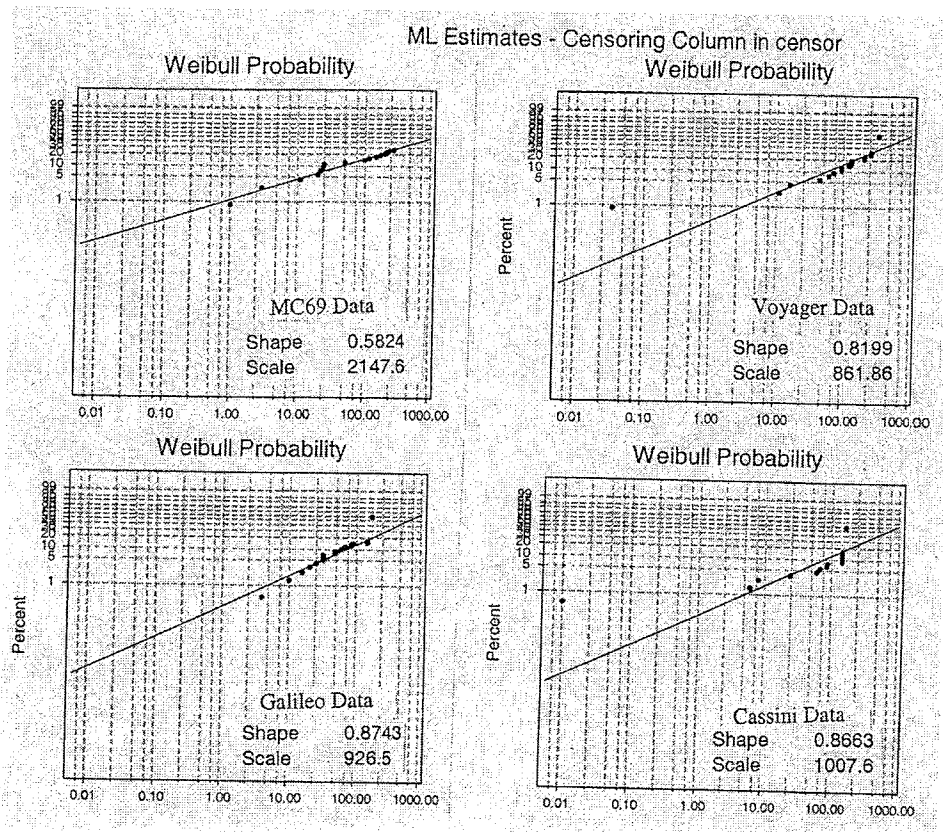


Figure 5-2. Rates of Change of Hazard Functions of S/C Assemblies

The results show that the assemblies have similar shape and scale factors as follows:

Spacecraft	Mariner69	Voyager77	Galileo89	Cassini97
Shape Factor	0.5824	0.8199	0.8743	0.8663
Scale Factor	2147.6	861.86	926.50	1007.6

The mean time to failure, standard deviation, median, inter-quartile range, and the Anderson & darling goodness-of-fit indicator of each set of data are shown in Table 5-2.

Table 5-2. Weibull Parameters for Spacecraft Assembly Test Failures

Parameters	Mariner69	Voyager77	Galileo89	Cassini97
Shape factor, β	0.5824	0.8199	0.8743	0.8663
Scale factor, η	2147.6	861.86	926.5	1007.6
MTTF	3363.1	959.96	990.96	1083.5
Standard Dev	6138.5	1178.6	1136.7	1254.9
Median	1144.5	551.17	609.24	660
IQR	3510.1	1095.1	1123.3	1229.8
Anderson-Darling	230.14	49.672	85.291	77.203

The calculated hot dwell test durations based on the same rate of change of hazard function as before are as follows:

<u>Spacecraft</u>	<u>Mariner69</u>	<u>Voyager77</u>	<u>Galileo89</u>	<u>Cassini97</u>
dh/dt (1/hr ²)	-6.01E-6	-6.00E-6	-6.0850E-6	-5.91.0E-6
τ_{dwell} (hrs)	76	48	30	31

6. Molecular Venting

Spacecraft flight assemblies should have vent hole(s) or vent path(s) in order to achieve the following objectives:

- (1) Low (Δp)'s: The vent holes should assure that the assemblies with thin walls experience only very low (Δp)'s across the containing walls so that high stresses and/or "ballooning" do not occur during launch phase of the mission or during pumpdown period of the thermal vacuum testing.
- (2) Fast Vent Speed: For radio frequency and microwave assemblies, the venting provision should assure that the entrapped air inside the assembly escapes to its surroundings with sufficient speed so that multipacting or ionization breakdown is not a concern during launch or testing.

- (3) Low Rate of Outgassing: The venting provision should ascertain that the entrapped gas escapes sufficiently fast so that the remaining gas does not contribute significantly to the unwanted small-force disturbances for altitude and attitude control and operation of the spacecraft in space.

Verification of venting design is accomplished by a combination of analysis and (partial) testing. Venting analysis should be performed in two steps:

- For the continuum regime of the flow (from ambient to 10^{-5} torr condition), one-dimensional transient flow analysis is usually adequate. Heat transfer and friction losses at the vent hole(s) are usually neglected but compressibility must be included in this analysis.
- Following the one-dimensional continuum flow analysis, a molecular venting analysis is performed. A particular example is offered below and as shown in Figure 6-1.

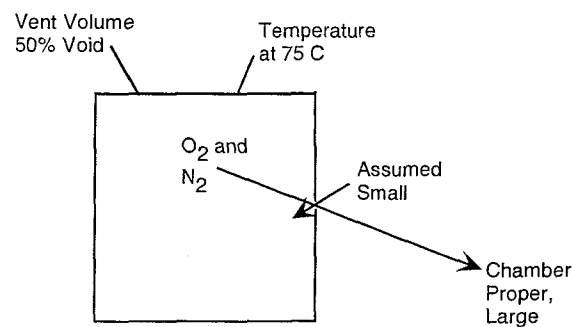


Figure 6-1. Molecular Venting

The overall configuration for this example is:

Gas = Air
 Assembly volume = 12'' x 12'' x 12''
 Void = 50 %
 Vent hole diameters = 0.005''

The initial number density is calculated as follows:

$$n_i = p_i / (k T J) \sim 3 \times 10^{17} \text{ molecules/m}^3 \text{ (Equation of State, Ideal Gas)}$$

where p_i = Initial pressure = 10^{-5} torr = 1.333 N/m^2 (end of pumpdown)
 k = Boltzmann constant = 1.3803×10^{-23} joules/molecule °K
 T = Hot dwell test temperature = $75 \text{ °C} = 348 \text{ °K}$

$$J = \text{Heat/Work conversion} = 10^7 \text{ cm-dyne/joules}$$

The number flux at vent opening, namely, the number of collisions with the wall per unit time per unit area, is [10]:

$$(V)(d^2n/dtdA) = (1/4)(n)(v)$$

where n is number density at time t (molecules/m³), t is time (s), V is vent volume (m³), A is vent area (m²), and v is mean molecular velocity (m/s).

The rate of number reduction inside the vent volume (after integrating with respect to the area A) is:

$$dn/dt = -(1/4)(nvA/V)$$

and the number densities are (after integrating with respect to t):

$$n/n_i = e^{-0.0001117t} \text{ (for vent hole size 0.005 inch, } t \text{ in seconds)}$$

$$n/n_i = e^{-0.0004455t} \text{ (for vent hole size 0.010 inch, } t \text{ in seconds)}$$

The number densities as a function of time are shown graphically in Figure 6-2. It can be concluded that:

- (1) After pumpdown, gas molecules will vent through the vent hole via molecular motion.
- (2) Number density in the volume decreases exponentially.
- (3) Number density in the vent volume decreases fast when the vent hole is sufficiently large. It drops to 5 % of the initial value in 2 hours when the hole is 0.010" in diameter (Figure 6-2). When the hole size is small, however, the number density can remain significant high, like 5.0E15 molecules/m³ at 10 hours when the hole size is 0.005" (Figure 6-2).
- (4) When number density is important for performance reasons, a vent analysis of the type as shown above should be performed and the size of vent hole can be finalized.
- (5) 20 hours can be considered as a thermal vacuum hot dwell test duration when there is no particular tailoring for molecular venting.

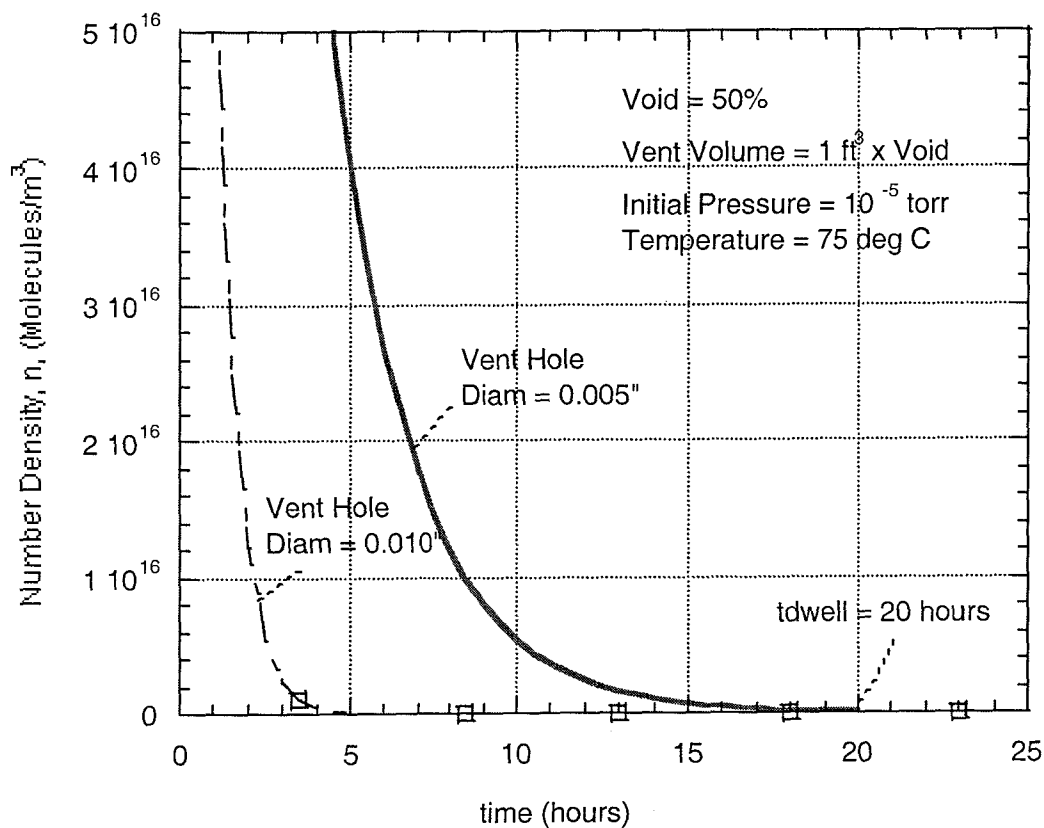


Figure 6-2. Number Density vs. Time for Molecular Venting

7. Outgassing

David, Freeman, and Zeiner [11, 12,13] have shown that, when the reaction rate kinetics is of the order 1, the outgassing material leaves a surface (Figure 7-1) with a rate according to:

$$dw/dt = -kw$$

where w = weight or mass being outgassed (grams)

t = time (hours)

k = rate constant for a particular outgassing configuration (hour⁻¹)

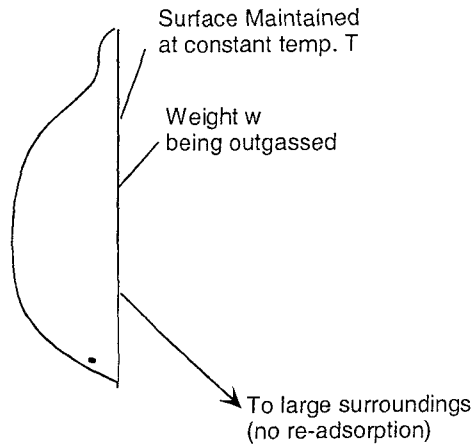


Figure 7-1. Material Outgassing

The dependence of the outgassing rate on the activation energy and temperature is embedded in the rate constant, k :

$$k = Ae^{-E/RT}$$

where A = an experimental constant (hour^{-1})

E = activation energy (cal/mole)

R = universal gas constant (i.e., 1.986 cal/mole-°K)

T = absolute temperature (°K)

Rate of Outgassing

For a certain outgassing scenario, such as for an assembly-level thermal vacuum hot dwell test, A , E , R , and T are all physical constants or actively maintained at a constant value. k , therefore, is a constant. The rate equation is, then, readily integrable; that is,

$$w/w_0 = e^{-kt}$$

where the current outgassing weight is w and $w = w_0$ at $t = 0.0$, w_0 being the initial weight. The rate of outgassing (normalized by the initial weight w_0) is, therefore:

$$(1/w_0)(dw/dt) = -ke^{-kt}$$

It is seen that that outgassing rate decays exponentially.

Weight Outgassed

When the weight outgassed, $w_0 - w$, is expressed in fractions of the initial weight w_0 , it takes on a simple form as follows (directly from $w/w_0 = e^{-kt}$):

$$\Phi = (w_0 - w)/w_0 = 1 - e^{-kt}$$

where w of the current outgassing weight (or the remaining weight) and Φ is the weight fraction already outgassed. The current time is t .

Outgassing rate data of Hughes [14], Allen [15], and Henderson [16] for:

- Teflon
- Aluminum Tape and Solar Cell Adhesive
- S13GLO paint
- Chemglaze Z306, Penzane, and Initial Surface Contamination
- RTV 566
- Polydimethylsiloxanes

are shown in Table 7-1. The rate data range from 4.4×10^{-29} 1/hour for Teflon to 16.2 1/hour for RTV 566 and Polydimethylsiloxanes.

Table 7-1. Outgassing Parameters (Reaction Order of 1) [14], [15], [16]

Material	A (1/s)	E (Kcal/mole)	T (K)	k (1/hour)	k corrected for T = 75 C(1/hour) (6)
<u>Teflon</u> (2)	4.73×10^{18}	80.5	398 (125 C)	1.0×10^{-22}	4.4×10^{-29}
Aluminum Tape Solar Cell Adhesive	-	-	-	-	0.001 (4)
S13GLO Paint	-	-	-	-	0.020 (4)
Chemglaze Z306, Penzane, Initial Surf. Contaminates	-	-	-	-	0.080 (4)
RTV 566	1.0×10^{13} assumed	24.85 Calc'd	323 (50 C)	0.539	16.17
<u>Polydimethyl- siloxanes</u> (3)	1.0×10^{13} (5)	$22.26M + 4387$ (M = Mol. Wt. = 900)	373 (100 C)	173	16.2

Notes for Table 7-1:

- (1) A=Proportional Constant, E=Activation Energy , T=Temperature , k=Rate constant ,
R =Universal Gas Constant = 1.986 cal/mole-°K
- (2) Reference: T. A. Hughes [14].
- (3) Reference: T. H. Allen [15].
- (4) Reference: K. Henderson [16].
- (5) A in this case is assumed to be 1.0×10^{13} (1/s).
- (6) Assuming A and E do not change when making adjustment for temperature:

$$k_2 = k_1 e^{-(E/R)(1/T_2 - 1/T_1)}$$

The rate of outgassing and the weight outgassed as a function of time are calculated and shown in Figure 7-2 a and b. The results show that RTV566 and polydimethylsiloxanes outgas very rapidly. Chemglaze Z306, Penzane, and initial surface contamination outgas practically completely in 60 hours. S13GLO paint, aluminum tape, solar cell adhesives, and Teflon, however, all take a very long time to outgas.

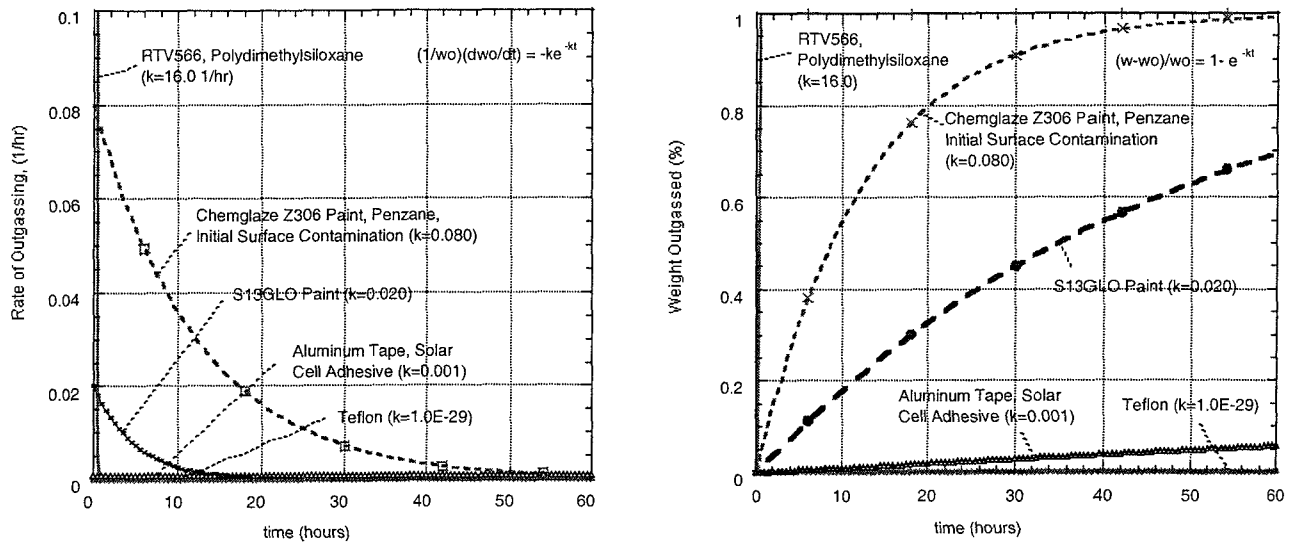


Figure 7-2 a,b. Outgassing Rates and Weights Outgassed

8. Curing

Phases of the Curing (Thermosetting) Process

The test data of rubber modified epoxy of M. Doyle [17] are shown in Figure 8-1. The data clearly shows three rheological phases for the curing process:

- (1) Fluid Phase - A phase characterized by a liquid state of the adhesive with zero shear strengths
- (2) Gel/Rubbery Phase - An intermediate transition phase from fluid to glass state
- (3) Glass Phase - A glass-like state showing highest joint strength and signifying the completion of the curing process

At lower curing temperatures, the adhesive goes through the full three phases of the curing process, fluid, gel/rubber, and glass. At high curing temperatures (125 °C and above), however, the adhesive does not reach the glass phase at all and, if the curing temperature is too high, may incur severe degradation. The latter is a condition to be avoided in actual practice.

Curing Curves and Glass Transition Times

The “curing curves” are shown in Figure 8-1 as “isothermal process lines” labeled with the curing temperatures of 50 °C, 75 °C, 100 °C, etc. according to the temperature at which curing took place.

The curing curves in Figure 8-1 exhibit two important times of the curing process:

τ_1 , the start time of the transition to glass phase
(when the curing curve starts to rise sharply)

τ_2 , the end time of the transition to glass phase
(when the curing curve becomes level again)

The following definitions can be derived from τ_1 and τ_2 :

$$\text{Glass Transition Period} = \tau_2 - \tau_1$$

$$\text{Mean Glass Transition Temperature} = (T(\tau_1) + T(\tau_2)) / 2$$

“Glass Temperature”, T_g = The mean glass transition temperature when τ_1 and τ_2 become the same; or the highest mean glass transition temperature in Figure 8-1.

“Glass transition line” is the locus (or the connecting line) of the mean glass transition temperatures, shown as a broad solid line in Figure 8-1.

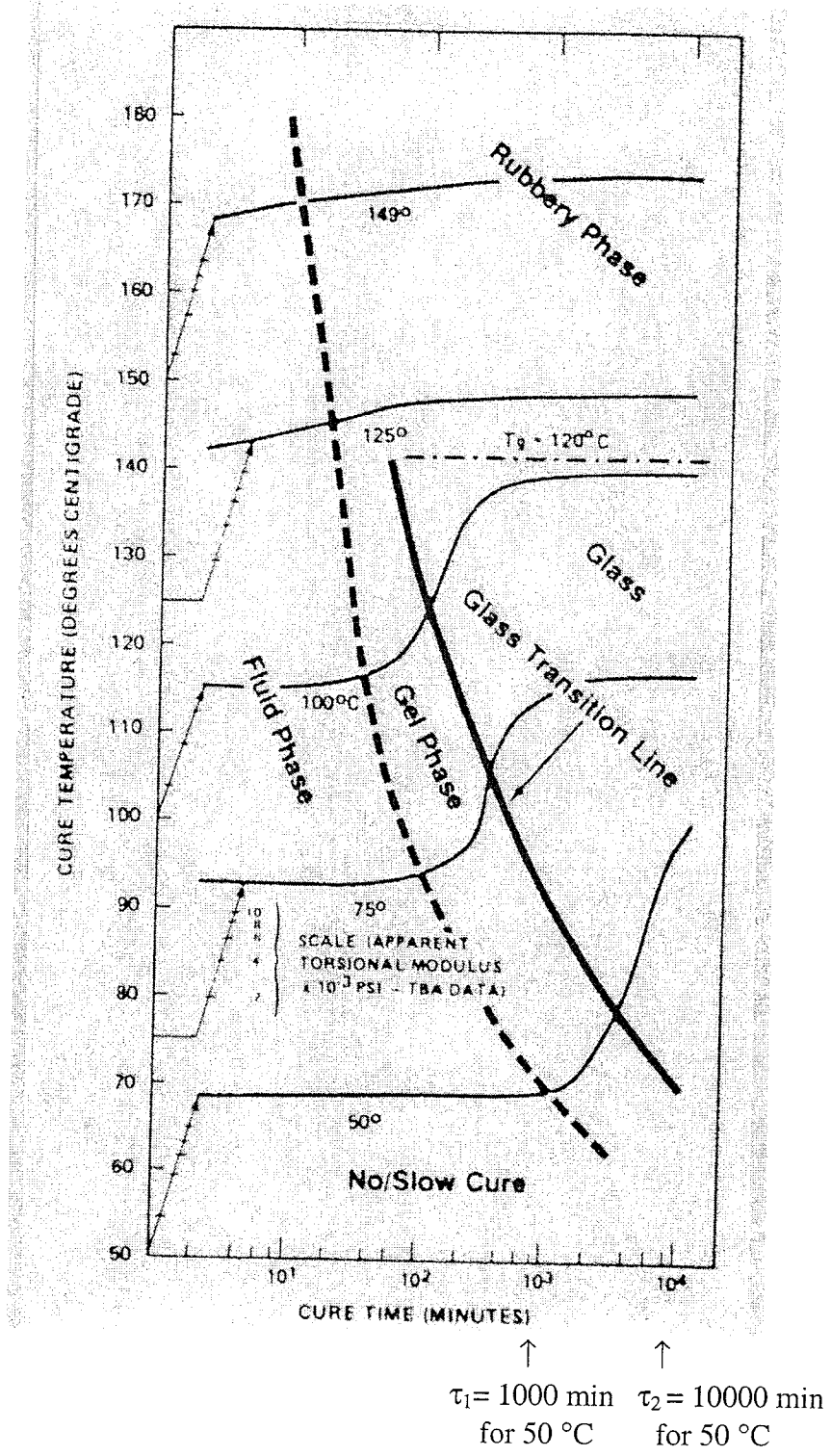


Figure 8-1. Phases of the Curing Process, Curing Curves, and Glass Transition Times τ_1 and τ_2 of FM-73 [17]

The glass transition times and the mean glass transition temperatures of FM-73 as measured by M. Dolye [17] are taken from Figure 8-1 and shown in Table 8-1 below:

Table 8-1. Glass Transition Temperatures and Times of FM-73

Curing Temp.	Classification Start Time τ_1	Classification End Time τ_2	Mean Glass Transition Temp.
50 °C	1000 Min	10000 Min	77 °C
75 °C	60 Min	2000 Min	108 °C
100 °C	10 Min	1000 Min	125 °C

The “Glass Temperature”, T_g , as read from Figure 8-1 is 140 °C, which is corrected to be 120 °C [17].

It is seen from Figure 8-1 that the general behavior of curing of epoxy can be described as [17]:

“Curing proceeds with a rate which increases with the curing temperature”.

Adhesive Joint Strengths

The ultimate goal of the adhesive is to maximize the joint strength which bonds the elements being joined. The joint strengths of FM-73 were measured according to the procedure “Lap Shear ASTM D-1002, Aluminum/aluminum” by M. Doyle [17].

The joint strengths of FM-73 cured at 100 °C are shown in Table 8-2 below:

Table 8-2. Adhesive Joint Strengths of FM-73, Aluminum/Aluminum, Based on cohesive type of joint failures [17]

Curing Condition	Joint Strength
1.5 hours at 100 °C	4200 psi
20 hours at 100 °C	4900 psi

The test data were obtained on commercially available materials. Adhesives were supported on thin polyester fiber matt. The joint strengths represented the average of at least 6 test specimens.

It is noted that an increase of curing time of from 1.5 hours to 20 hours (an 18.5 hours additional curing) translates into an increase of the joint strength of about 17% (i.e., 700 psi/4200 psi).

Curing Behavior of FM-73 Relevant to Hot Dwell Testing

The following conclusions can be drawn for FM-73 based on the test data of Reference 17:

- (1) At very low temperatures, FM-73 “freezes” and very little curing occurs.
- (2) At 50 °C, the glassification of FM-73 starts at 1,000 minutes (the 17th hour) and completes at 10,000 minutes (167th hour) - a fairly long time.
- (3) Very little degradation of FM-73 occurs when curing is performed below the glass temperature of 120 °C.
- (4) At 75 °C, glass transition (curing) of FM-73 starts at 1.7 hours and completes at 33.3 hours.
- (5) Joint strength is gained for longer cure time. At 100 °C, 17% is gained with an increase of curing time of 18.5 hours.

The data of Reference 17 shows that, for consideration of the curing of epoxy adhesives, the assembly-level thermal vacuum hot dwell test at 75 °C should be at least 30 hours in duration.

9. Stress Relaxation

Given time, solid material under sustained stress loading shows a gradual “flow” of the material – a phenomenon known as creep. In metal, creep can be defined as the plastic deformation resulting from the slips of the crystals in the crystallographic direction and is oftentimes accompanied by some flow of the grain boundary materials. The “bulging” of the flat-surfaced fillets of a solder after repeated thermal cycling is the result of creep. Creep, by definition, is largely non-recoverable.

In electronics, solder, a low-melting-point metal, is used extensively. The creep behavior of solder is, therefore, very important for sound design and reliability. The creep behavior of solder is a strong function of [19, 20]:

- (1) The loading condition (i.e., the stress level);
- (2) The grain size of the solder;
- (3) The metallurgical state of the solder (i.e., as-cast, superplastic, or coarsened);
- (4) The temperature of the solder; and
- (5) The board, solder, lead, and combined stiffnesses.

The creep behavior of solder is typically described in terms of the “rate of creep strain” as a function of the stress loading. The experimental data of various investigators are shown in Figure 9-1. The non-linearity, the three regions of strain rates (plastic deformations), and the effect of the metallurgical states are all very clear.

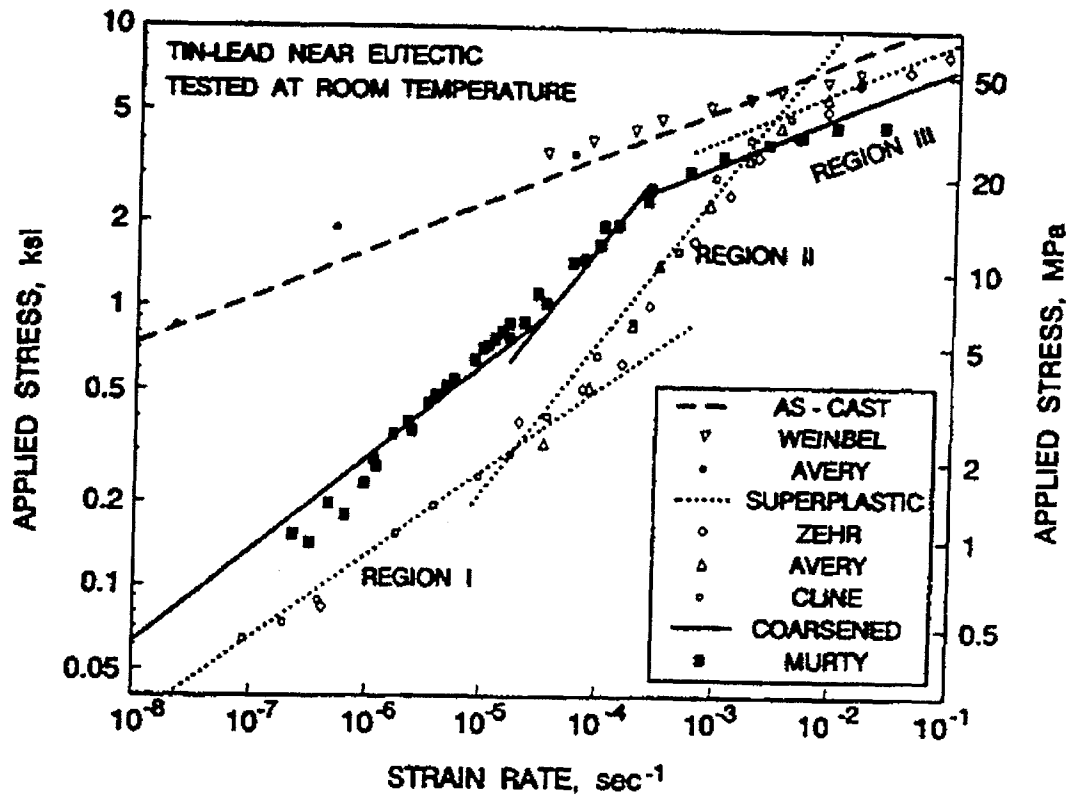


Figure 9-1. Behavior of the Creep of Solder : The Rate of Creep Strain as a function of The Stress Loading (Weinbel, Avery, Zehr, Cline, and Murty)

It has been shown that the creep behavior of solder can be expressed as a power relationship between the rate of creep strain and the time-varying stresses (or as a hyperbolic-sine law [21]) as follows:

$$d\varepsilon/dt = \sigma^n g^{-p} e^{-E_a/(kT)}$$

where t = time (sec)

ε = the creep strain, i.e., the deformation of the solder (%)

$d\varepsilon/dt$ = the rate of strain of the solder (1/second)

$\sigma = \sigma(\tau)$ = solder stress, a function of time

n = creep exponent (typically 2 to 3)

g = grain size

p = grain size exponent (typically 1.6 to 2.3)

E_a = thermal activation energy of creep

k = Boltzmann constant

T = solder temperature (K)

The effects of stresses, grain size, and temperature are all combined into one expression.

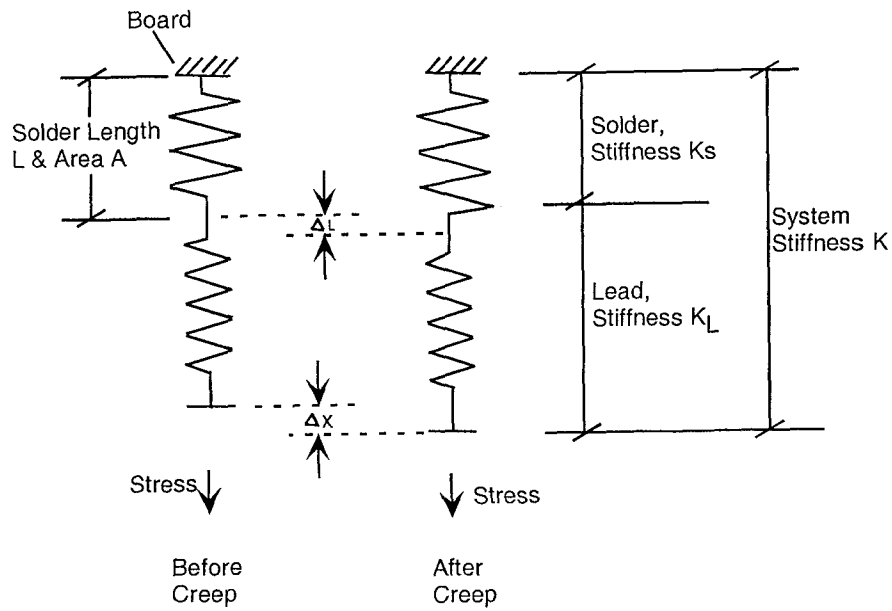


Figure 9-3. Modeling of the Board-Solder-Lead System : The Stiffnesses K 's
 (Permit by Author of Reference 19)

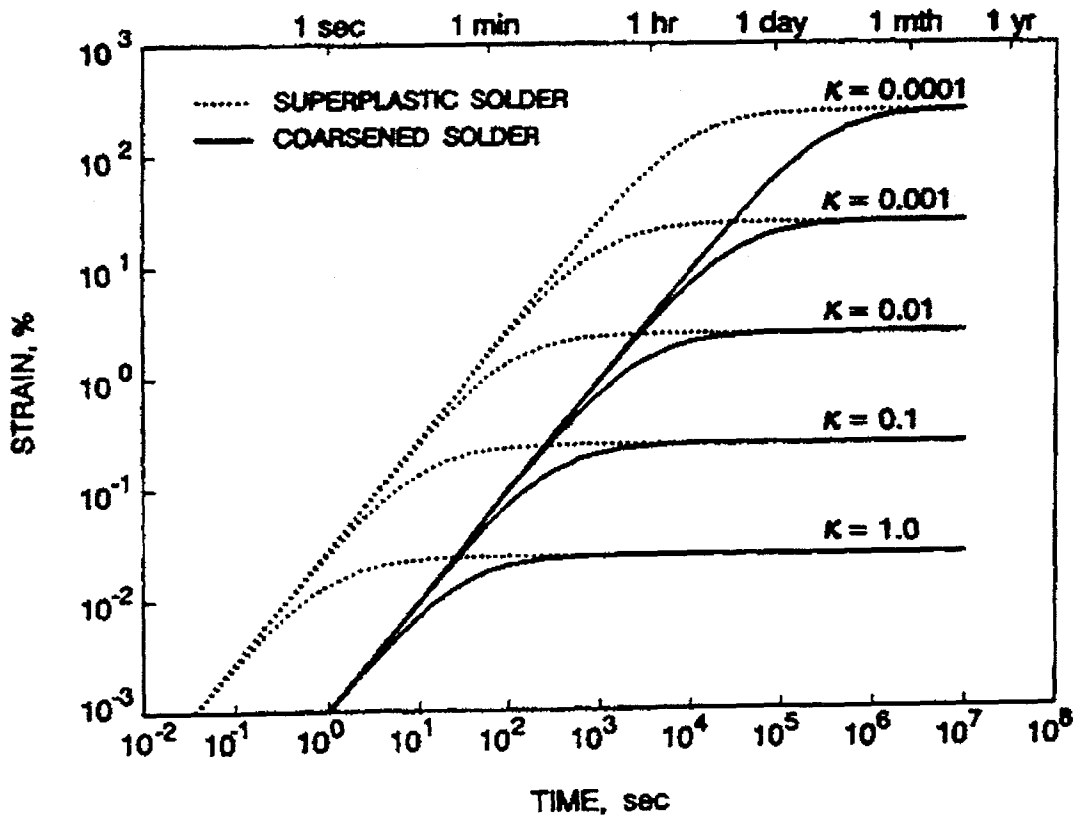


Figure 9-4. Creep Behavior of a Board-Solder-Lead System with Initial Loading of 1 ksi (Reprint by Permission from the Author of Reference 19)

Table 9-1. Time to Complete Stress Relaxation based on Ref. 19

Relative Stiffness, κ	Time to Complete Stress Relaxation	
	Seconds	Hours
1.0	$3.0 \times 10^{+2}$	0.08
0.1	$3.0 \times 10^{+3}$	0.8
0.01	$3.0 \times 10^{+4}$	8.0
0.001	$3.0 \times 10^{+5}$	80.0
0.0001	$3.0 \times 10^{+6}$	800.0

10. Conclusions and Recommendations

A method of statistical modeling and reliability analysis of the parts and assembly test failure data is introduced. Based on the results from such analysis, a criterion to arrive at the proper duration of thermal vacuum hot tests is suggested.

This methodology is applied to the parts of recent applications (Vishay-Sprague tantalum capacitors and CMOS integrated circuits) and assemblies from four spacecrafts (Mariner69, Voyager77, Galileo89, Cassini97) and the hot dwell test durations are derived.

Four physical phenomena:

- Molecular Venting
- Material Outgassing
- Material Curing
- Stress Relaxation

were studied as they were related to the duration of a hot dwell test.

The results show that, in order for the rate of change of hazard function to reach below $-6.0E-06$ 1/hour² or for the physical processes to reach 99% completion, the hot dwell test durations show a range from the low of 29 hours for the test data of tantalum capacitors to the high of 80 hours from the physics of stress relaxation as shown in the following table. These test durations are seen to be consistent with those used by NASA Centers and six aerospace companies based on Reference No. 22 survey.

<u>Method</u>	<u>Hardware/Physics</u>	<u>Hot Dwell Test Duration (Hours)</u>
Reliability	Parts (Capacitor)	25
	Parts (CMOS ICs)	57
	Assemblies (Mariner69)	76
	Assemblies (Voyager77)	48
	Assemblies (Galileo89)	30
	Assemblies (Cassini97)	31
Physics	Molecular Venting	20
	Material Outgassing	60
	Epoxy Curing	30
	Stress Relief	80

Based on the results of this study, it appears reasonable to adopt a procedure for the hot dwell test duration as follows:

- (1) There be a requirement for a minimum duration (hours) for a hot dwell test of spacecraft assemblies.
- (2) Without special tailoring, the minimum hot dwell test duration be 80 hours based on the process of stress relaxation.
- (3) In tailoring the duration of the hot dwell test, the assemblies be grouped according to their design and intended usage as follows:

Electronics
 Motors, Actuators, Mechanisms
 Instruments (Sciences)
 Propulsion Components
 Optics
 Antenna
 Solar Arrays
 Batteries
 New or Developmental Assemblies

and the proper hot dwell duration be determined according to their respective data analysis, failure physics, heritage, and past experience.

- (4) For the reliability and survivability analysis, the unavailability of failure data leads the field of obstacles. The difficulty lies with the mentality: "My hardware does not fail. So I have no failure data". This is not realizing that failure data can be positive and valuable information which will lead to the truth of the matter eventually. For future progress, it is suggested that test data be taken properly. In addition to describing the failure physics and plan of corrective actions, the recorded data is to include at least:

- Start time of the hot test phase
- Failure time (i.e, the time from the start of hot test phase when the failure actually occurs)
- End time of the hot test phase
(Similarly for the Cold test phase)

and the failure data be distributed to all interested parties, internally as well as externally.

It is hoped that this work offers a way of analyzing failure data and a method to arrive at the proper duration of a hot dwell test. It is hoped that efforts of test failure data collection, analysis, and distribution are continued in the future.

11. References

1. Minitab, Inc., "Minitab Statistical Software", Release 13 for Windows 2000
2. Trevedi, K. S., 1982, "Probability and Statistics with Reliability, Queuing, and Computer Science Applications", Duke University, Prentice-Hall
3. Ebbeler, D., 23 February 2001, JPL Interoffice Memorandum, "Mars 01 UHF Transceiver Reliability Analysis"
4. MIL-PRF-55365D, Amendment 2, 9 November 2000, "Capacitor, Fixed, Electrolytic (Tantalum), Chip, Non-established Reliability, Established Reliability, General Specification for"
5. Scheuer, E., Aug 7, 1991, JPL Interoffice Memorandum No. 91-446, "Life Analysis of Philips Resistor"
6. Boyko, K. C., and Gerlach, D. L., 1989, "Time Dependent Dielectric Breakdown of 210 Angstrom Oxides", CH2650-0/89/0000-0001\$01.00 C, IEEE/IRPS
7. Buehler, M., Zamani, N., and Zoutendyk, J., March 1992, "CMOS-ASIC Life-Predictions from Test-Coupon Data", Proc. IEEE 1992 Int. Conference on Microelectronics Test Structures, Vol. 5
8. Automated Problem/Failure Report System, Test Result Summary Forms, JPL
9. Fu, J., Personnel Files, JPL
10. Lee, J. F., Sears, F. W., and Turcotte, D. L., 1963, "Statistical Thermodynamics", Addison-Wesley Publishing Co.
11. David, C., 1975, "Thermal Degradation of Polymers", Comprehensive Chemical Kinetics, Vol. 14, Degradation of Polymers, C. H. Bamford and C.F.H. Tipper (ed.), pp. 28-32, Elsevier Publishing Co., N.Y.
12. Freeman, E.S., and B. Carrol, 1958, "The Application of Thermoanalytical Technique to Reaction Kinetics", The Thermogravimetric Evaluation of the Decomposition of Calcium Oxalate Monohydrate, J. Phys. Chem., 662, 394-397.
13. Zeiner, E. A., "A Multinodal Model for Surface Contamination Based Upon the Boltzmann Equation of Transport"

15. Allen, T. H., Hughes, T. A., Lt. Price, B. C., Nov. 1975, "A Study of Molecular Contamination", Proceedings IES/AIAA/ASTM/NASA Eighth Space Simulation Conference (NASA SP-379)
16. Henderson, K., 3 April 1992, TRW Space and Defense FSCM No. 11982, "Total Ozone Mapping Spectrometer Earth Probe, Contamination Sources and Effects Analysis"
17. Doyle, M., Li, H. M., and Lewis, A. F., Mid-August 1979, "Time-Dependent Cure Behavior of Epoxy Based Structural Adhesives", Polymer Engineering and Science, Vol. 19, No. 10
18. Forsberg, G., July 19, 2001, Personal communication with
19. Ross, Jr., R. G., Wen, L. C., and Mon, G. R., June 1993, "Solder Joint Creep and Stress Relaxation Dependence on Construction and Environmental-Stress Parameters", Journal of Electronics Packaging, Vol. 115, Pages 165-172
20. Ross, Jr., R.G., June 1991 "A system Approach to Solder Joint Fatigue in Spacecraft Electronic Packaging", Journal of Electronic Packaging, Transaction of the June 1991, Vol. 113, Page 121-128
21. Pan, T.Y., March 1991, "Thermal Cycling Induced Plastic Deformation in Solder Joints – Part 1: Accumulated Deformation in Surface Mount Joints", ASME Journal of Electronic Packaging, Vol. 113, pp. 8-15
22. Fu, J., November 19, 1984, JPL Interoffice Memorandum, 5136-84-269, "Survey on Assembly Level Thermal vacuum Qualification Test Durations"